Evolution of the optical properties of chromium spinels $CdCr_2O_4$, $HgCr_2S_4$, and $ZnCr_2Se_4$ under high pressure

K. Rabia,[1] L. Baldassarre,[1] J. Deisenhofer,[2] V. Tsurkan,[2,3] and C. A. Kuntscher[1,*]

[1]*Experimentalphysik II, Universität Augsburg, Universitätstrasse 1, D-86159 Augsburg, Germany*

[2]*Experimentalphysik V, Universität Augsburg, Universitätstrasse 1, D-86159 Augsburg, Germany*

[3]*Institute of Applied Physics, Academy of Sciences of Moldova, MD-2028 Chisinau, Republic of Moldova*

(Received 18 October 2013; revised manuscript received 26 January 2014; published 10 March 2014)

We report pressure-dependent reflection and transmission measurements on $ZnCr_2Se_4$, $HgCr_2S_4$, and $CdCr_2O_4$ single crystals at room temperature over a broad spectral range 200–24 000 cm^{-1}. The pressure dependence of the phonon modes and the high-frequency electronic excitations indicate that all three compounds undergo a pressure-induced structural phase transition with critical pressures of 15, 12, and 10 GPa for $CdCr_2O_4$, $HgCr_2S_4$, and $ZnCr_2Se_4$, respectively. The eigenfrequencies of the electronic transitions are very close to the expected values for chromium crystal-field transitions. In the case of the chalcogenides, pressure induces a redshift of the electronic excitations, which indicates a strong hybridization of the Cr d bands with the chalcogenide bands.

DOI: 10.1103/PhysRevB.89.125107 PACS number(s): 61.50.Ks, 64.70.K−

I. INTRODUCTION

Chromium-spinel compounds with the formula ACr_2X_4, where A is a divalent nonmagnetic cation and X a divalent anion, exhibit many interesting phenomena such as strong geometric frustration, [1–3] relaxor multiferroicity, [4] or three-dimensional topological effects [5]. At room temperature these spinels are cubic (space group $Fd\bar{3}m$), where the nonmagnetic A-site ions are tetrahedrally coordinated and the Cr^{3+} ions (electronic configuration $3d^3$ with spin $S = 3/2$) in an octahedral environment form a pyrochlore lattice (see Fig. 1).

The inherent frustration of the pyrochlore lattice is often released by magnetoelastic interactions such as the spin-driven Jahn-Teller effect [6,7], which lead to a reduced structural symmetry coinciding with the onset of long-range magnetic order. The magnetostructural phase transition is reflected in the splitting of infrared- (IR) and Raman-active phonons and the crystal-field (CF) excitations, which are sensitive to changes in the magnetic and the crystalline symmetry [1,8–11]. Since magnetic interactions depend on interatomic distances [3], one can expect structural anomalies not only at low temperatures but also at high pressures.

In general, the application of pressure can be used to tune in a controlled fashion the electronic and structural properties of a system, while optical spectroscopy is a powerful method to investigate the electronic and vibrational properties of a material. The combination of the two techniques thus allows one to follow the evolution of the phonon frequencies and the (possible) splitting of optical phonon modes with applied pressure, providing useful information on both the magnetic [9,12,13] and structural properties. The far-infrared studies on the spinel compounds can indeed reveal information on the structural properties (e.g., cation ordering, bond strengths, and ionicities), on the free carrier contribution, and on magnetic phenomena [14].

Earlier work on the pressure effects in chromium spinels has concentrated on alterations of the crystal structure [3,15]. In this paper we focus on the effect of pressure on the optical properties of $ZnCr_2Se_4$, $HgCr_2S_4$, and $CdCr_2O_4$ spinels in a broad frequency range (200–24 000 cm^{-1}) at room temperature. Based on the pressure dependence of the phonon modes and the electronic excitations, we propose the occurrence of a pressure-induced structural phase transition in all three compounds.

The paper is organized as follows: In Sec. I we discuss the experimental details of the pressure measurements and the data analysis procedure. We present the obtained optical spectra in Sec. II, discuss the results in Sec. III, and summarize our findings in Sec. IV.

II. EXPERIMENT

We have investigated the three single-crystalline Cr spinels $ZnCr_2Se_4$, $HgCr_2S_4$, and $CdCr_2O_4$ by means of infrared reflection and transmission measurements under pressure in the frequency range 200–24 000 cm^{-1}. The single crystals of $ZnCr_2Se_4$ and $HgCr_2S_4$ were grown by chemical transport reactions [1,16], and $CdCr_2O_4$ was grown by a flux method.

The pressure-dependent reflectivity and transmission measurements were performed at room temperature, using a Bruker IFS 66v/S Fourier transform infrared (FTIR) spectrometer. Far-infrared (FIR) reflectivity measurements were carried out at beamline IR1 of ANKA. The higher-frequency measurements were carried out with conventional infrared radiation sources. A Syassen-Holzapfel diamond anvil cell (DAC) [17], equipped with type IIa diamonds suitable for infrared measurements, was used to generate pressures up to 20 GPa.

A Bruker IR ScopeII infrared microscope with a 15× magnification objective coupled to the spectrometer was used to focus the infrared beam onto the small sample in the pressure cell. The samples were mechanically polished down to a thickness of ≈50 μm and a small piece of the sample (about 80 μm × 80 μm in size) was cut and loaded, together with CsI powder as the pressure medium, in a 150 μm diameter hole drilled in a stainless steel gasket. Great care was taken when loading the sample, in order to obtain a

*christine.kuntscher@physik.uni-augsburg.de

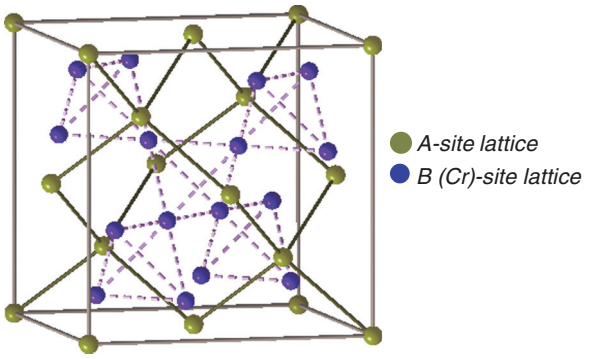

FIG. 1. (Color online) Illustration of A and B(Cr) sublattices in the cubic unit cell of normal spinels AB_2X_4. The tetrahedrally coordinated Cr atoms form a pyrochlore lattice.

clean and flat diamond-sample interface. With this crystal size and the corresponding diffraction limit, we were able to measure reliably in the frequency range down to 200 cm^{-1}. The ruby luminescence method [18] was used for *in situ* pressure determination. Variations in the synchrotron source intensity were taken into account by applying additional normalization procedures.

The measurement geometries are shown in Fig. 2. In the case of reflectivity measurements, spectra taken at the inner diamond-air interface of the empty cell served as the reference for normalization of the sample spectra. The absolute reflectivity at the sample-diamond interface, denoted as $R_{s\text{-}d}$, was calculated according to $R_{s\text{-}d}(\omega) = R_{\text{dia}}[I_s(\omega)/I_d(\omega)]$, where $I_s(\omega)$ denotes the intensity spectrum reflected from the sample-diamond interface and $I_d(\omega)$ is the reference spectrum of the diamond-air interface. $R_{\text{dia}} = 0.167$ was calculated from the refractive index of diamond n_{dia}. To obtain the transmittance spectrum, the intensity transmitted through the sample I_s was divided by the intensity transmitted through the pressure transmitting medium I_{ref}, i.e., $T(\omega) = I_s(\omega)/I_{\text{ref}}(\omega)$. The absorbance spectrum was calculated according to $A(\omega) = -\log_{10} T(\omega)$.

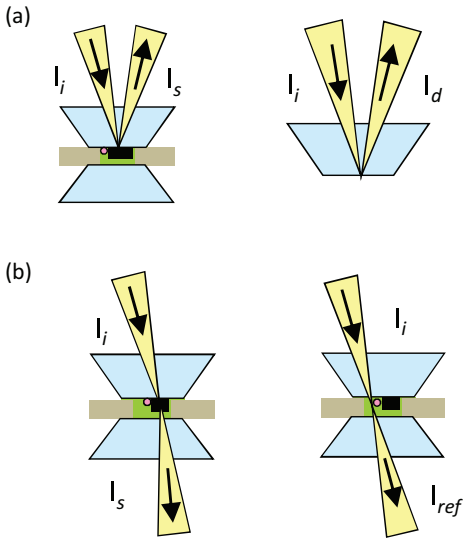

FIG. 2. (Color online) Measurement configurations: (a) Reflectance of a sample at the sample-diamond interface in a DAC and (b) transmittance of a sample in a DAC.

III. RESULTS

Reflectivity ($R_{s\text{-}d}$) spectra of $ZnCr_2Se_4$, $HgCr_2S_4$, and $CdCr_2O_4$ are shown for a few selected pressures in Figs. 3(a)–3(c) in the frequency range 250–24 000 cm^{-1}. The same curves are plotted separately in the low-frequency range [see Figs. 3(d)–3(f)] to better highlight the effect of pressure on the phonon modes. The region around 2000 cm^{-1} is cut out from the experimental spectra, due to strong diamond multiphonon absorptions that cause artifacts in this spectral range. A linear interpolation has been performed in this range in order to perform the analysis.

For the analysis of the reflectivity data, we applied the Lorentz model, where the complex dielectric function is defined as [19]

$$\epsilon(\omega) = \epsilon_\infty + \sum_j \frac{\Delta\epsilon_j \omega_{\text{TO}_j}^2}{\omega_{\text{TO}_j}^2 - \omega^2 + i\omega\gamma_j}. \quad (1)$$

In this model each mode is characterized by three parameters: the oscillator strength $\Delta\epsilon_j$, the frequency of transverse optical modes ω_{TO_j}, and the damping of the modes γ_j. The fits along with the measured reflectivity spectra are shown in Fig. 3 as red dashed lines. The pressure dependence of the high-frequency permittivity ϵ_∞ used in our fitting was calculated according to the Clausius-Mossotti relation assuming ionic bonding [20], $\frac{\epsilon_\infty(P)-1}{\epsilon_\infty(P)+2} = \frac{\tilde{\alpha}N}{3\epsilon_0 V(P)}$, where $\tilde{\alpha}$ is the average atomic polarizability of the unit cell, obtained from the lowest-pressure data. $V(P)$ is the unit cell volume as a function of pressure calculated from the second-order Birch equation of state [21,22], $P(x) = \frac{3}{2}B_0 x^{-7}(1-x^2)$, where $x = [\frac{V(P)}{V(0)}]^{1/3}$. The value of the bulk modulus was assumed to be $B_0 =$ 100 GPa for $ZnCr_2Se_4$ and $HgCr_2S_4$, and $B_0 = 200$ GPa for $CdCr_2O_4$ based on x-ray diffraction data [3]. The obtained fit values were used for the extrapolation of the experimental reflectivity spectra to lower and higher frequencies necessary for the Kramers-Kronig (KK) analysis [23,24]. Since in the case of $HgCr_2S_4$ the reflectivity data are noisy below 1000 cm^{-1}, the fit was used to obtain the real part of the optical conductivity.

To examine the electronic excitations in the chalcogenide compounds, the real part of the optical conductivity was considered (see Fig. 4). The optical conductivity spectra for $ZnCr_2Se_4$ and $HgCr_2S_4$ at the lowest pressure reveal an insulating behavior, with two phonon modes in the low-frequency range (which are not shown in Fig. 4) and a strong absorption band at about 15 000 and 15 800 cm^{-1} for $ZnCr_2Se_4$ and $HgCr_2S_4$, respectively. Upon pressure increase these bands broaden and gradually shift towards lower frequencies.

For $CdCr_2O_4$ the reflectivity above ~5000 cm^{-1} is very low and exhibits only small changes under pressure [see Fig. 3(c)]. Therefore, additional transmission measurements were carried out on a single crystal of $CdCr_2O_4$ in the frequency range 8000–25 000 cm^{-1} up to 20.2 GPa, especially in order to follow the effect of pressure on the high-frequency excitations. In Fig. 5 the transmittance and absorbance spectra of $CdCr_2O_4$ are depicted for selected pressures. These spectra show a pronounced absorption band at around 16 760 cm^{-1} and weak

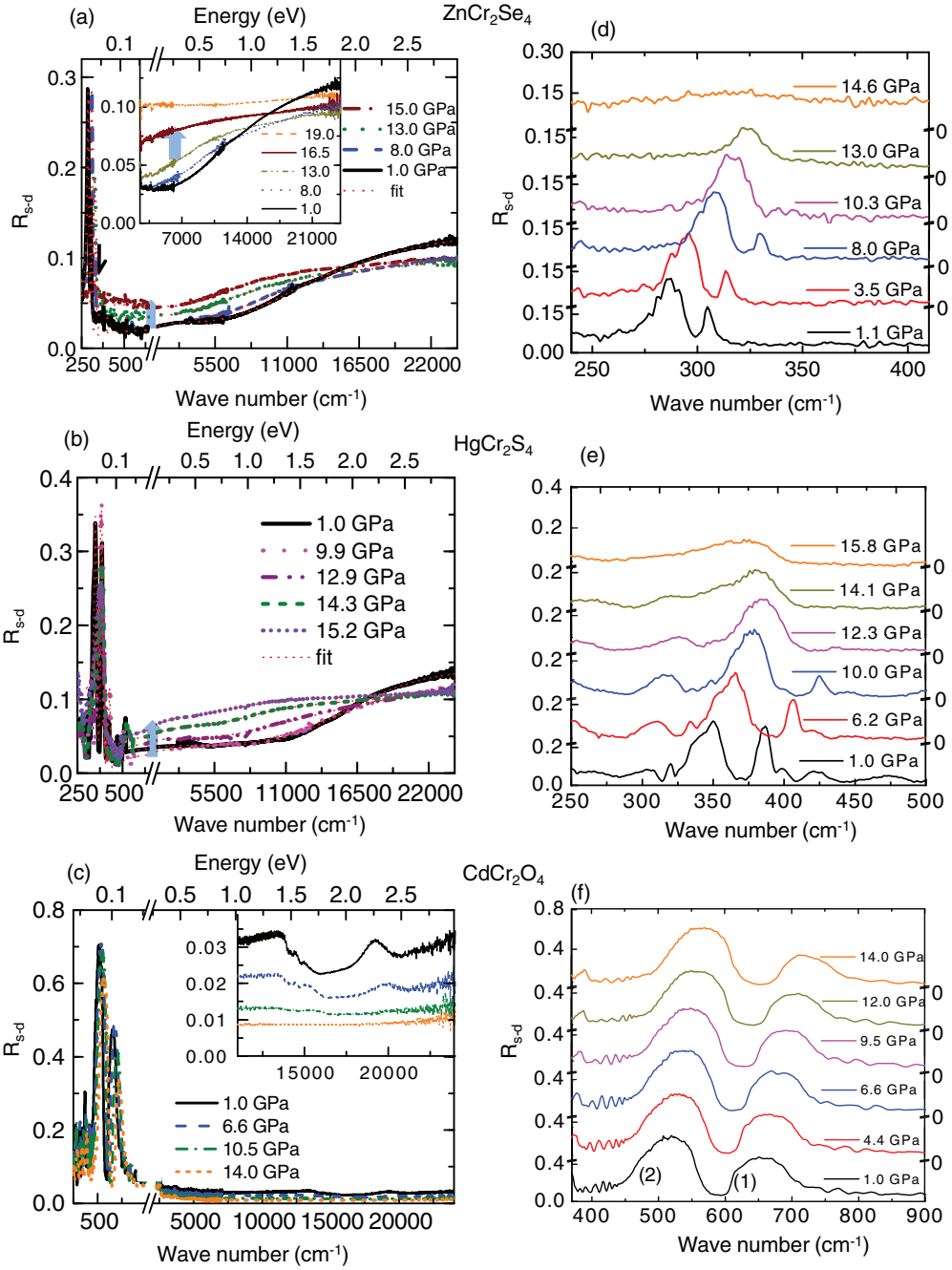

FIG. 3. (Color online) Room-temperature reflectivity $R_{s\text{-}d}$ spectra of (a) $ZnCr_2Se_4$, (b) $HgCr_2S_4$, and (c) $CdCr_2O_4$ in the spectral range 250–24 000 cm^{-1} for selected pressures. The red dashed lines are fits with the Lorentz model. In (a) the small feature at around 400 cm^{-1}, marked with a black arrow, is an artifact and not included in the fitting. Inset: Several selected $R_{s\text{-}d}$ spectra in the pressure range 1–19.0 GPa. In (c) the inset presents the magnification of the spectra in the frequency range 11 000–24 000 cm^{-1} to illustrate the very weak electronic excitations. The observed phonon modes of $ZnCr_2Se_4$, $HgCr_2S_4$, and $CdCr_2O_4$ are presented in (d)–(f), respectively. The spectra are offset for clarity. The screening of the phonon modes occur for $ZnCr_2Se_4$, and $HgCr_2S_4$ with increasing pressure, while in the case of $CdCr_2O_4$ the phonon modes remain intense up to the highest measured pressure.

features at 14 500 cm^{-1}. The high-frequency contributions to the absorbance spectra are shown in Fig. 6 for four selected pressures. The strong absorption band in $CdCr_2O_4$ exhibits a blueshift under pressure (see below for a quantitative analysis of the spectra).

In all three compounds a strong absorption band is observed at energies (see Table I) which are very close to the ones which have been attributed to spin-allowed intra-atomic d-d excitations (crystal-field excitations) [10,25–31]: The Cr^{3+} ion in an octahedral environment exhibits two spin-allowed crystal-field (CF) transitions, namely, from the $^4A_{2g}$ ground state to the $^4T_{2g}$ and $^4T_{1g}$ excited states. The transition from the ground state to $^4T_{2g}$ is located at 10 Dq (Δ_{oct}), where Dq is the Coulombic parameter of the ligand field. Usually, the

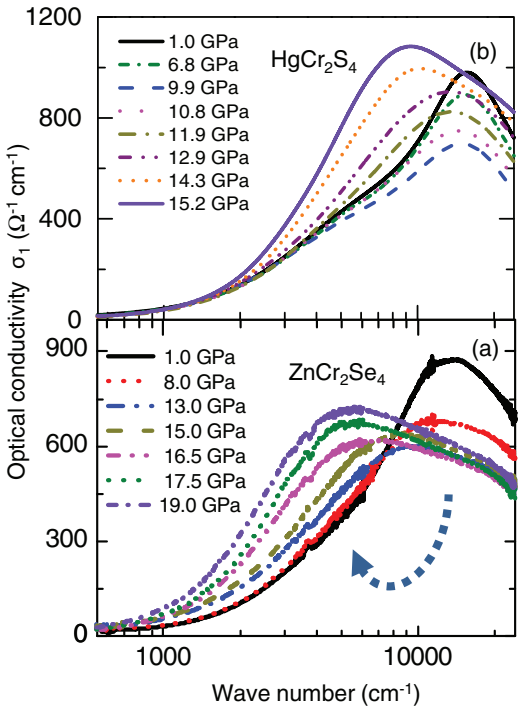

FIG. 4. (Color online) Real part of the optical conductivity of (a) $ZnCr_2Se_4$ and (b) $HgCr_2S_4$ for selected pressures. The arrow indicates the redshift of the electronic excitations.

CF transitions are parity forbidden because of the inversion symmetry at the transition-metal ion site. These transitions can become allowed by virtue of lattice vibrations, which locally break the center of symmetry [10,26,29]. This interpretation

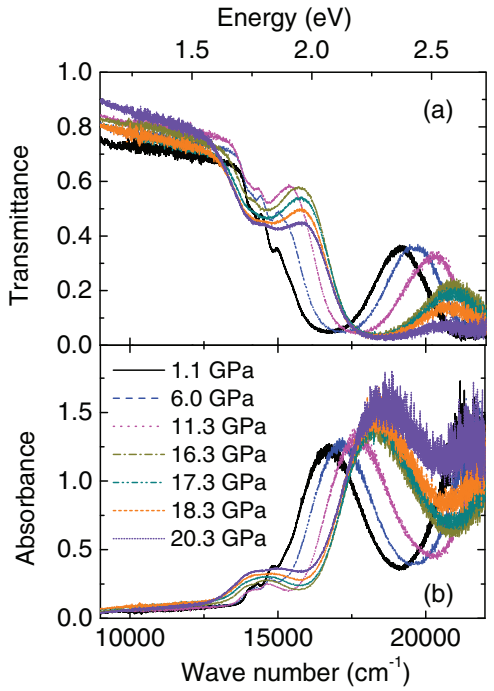

FIG. 5. (Color online) (a) Transmittance and (b) absorbance spectra of $CdCr_2O_4$ for several selected pressures.

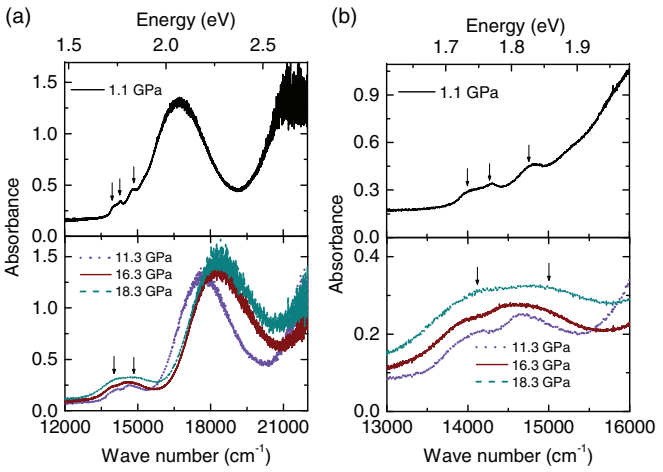

FIG. 6. (Color online) (a) Absorbance spectrum of $CdCr_2O_4$ at 1.1 GPa shows four features: one strong feature at ≈16 760 cm^{-1}, and three weak features marked with black arrows. At higher pressures (11.3, 16.3, and 18.3 GPa) only two low-energy absorption features marked with black arrows are resolvable. (b) Low-energy part of the spectra to illustrate the pressure dependence of the spin-forbidden transitions (marked with arrows).

is certainly fulfilled in the case of the oxide $CdCr_2O_4$, where these excitations can only be observed in transmission. With increasing pressure, the CF splitting is expected to increase, resulting in a blueshift of the CF excitations [32,33], in agreement with our findings.

The rather large oscillator strength of the corresponding electronic excitations in the chalcogenides can only be understood if strong hybridization effects occur between the chalcogenide p states and the chromium d states, and an interpretation of the pure CF transition is no longer adequate [34]. The mixed character of the electronic states for the chalcogenide may also explain the observed redshift under pressure in contrast to the blueshift observed for the oxide.

In Ref. [28] the center of gravity of CF excitations for many chromium complexes are given, where Cr^{3+} is in an octahedral environment. The energies of two spin-allowed transitions from the ground state $^4A_{2g}$ to the excited levels $^4T_{2g}$ and $^4T_{1g}$ vary from ≈13 000 to 17 000 and ≈17 000 to 22 000 cm^{-1}, respectively. The spin-forbidden transitions $^4A_{2g}$ to ^2E_g and $^2T_{2g}$ vary from 13 000 to 14 400 and 18 000 to 19 200 cm^{-1}, respectively.

Indeed, for $CdCr_2O_4$ weak features (marked by arrows) are observed at around 14 500 cm^{-1}, in addition to the strong absorption band. They are attributed to spin-forbidden transitions, which become allowed due to spin-orbit coupling [32]. At low temperature six spin-forbidden transitions can

TABLE I. The energies of the electronic transitions for the three investigated Cr-spinel compounds at ∼1 GPa.

Compounds	Frequency
$CdCr_2O_4$	16 760 cm^{-1}
$HgCr_2S_4$	15 800 cm^{-1}
$ZnCr_2Se_4$	15 000 cm^{-1}

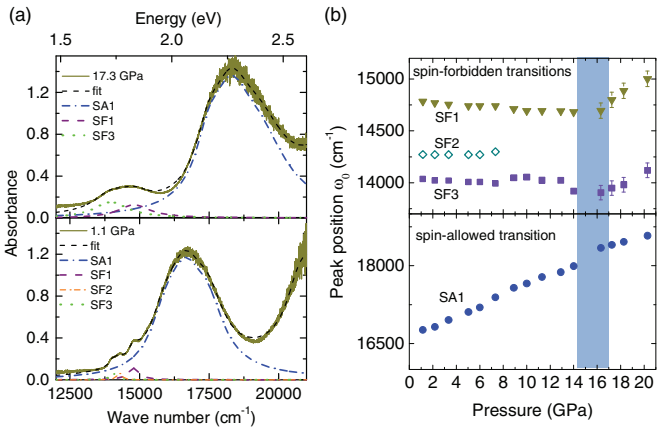

FIG. 7. (Color online) (a) Fit of the absorption spectrum of $CdCr_2O_4$ at 1.1 and 17.3 GPa consisting of four and three absorption features, respectively. (b) Peak position ω_0 of the absorption features as a function of pressure. The shaded area marks the transition region.

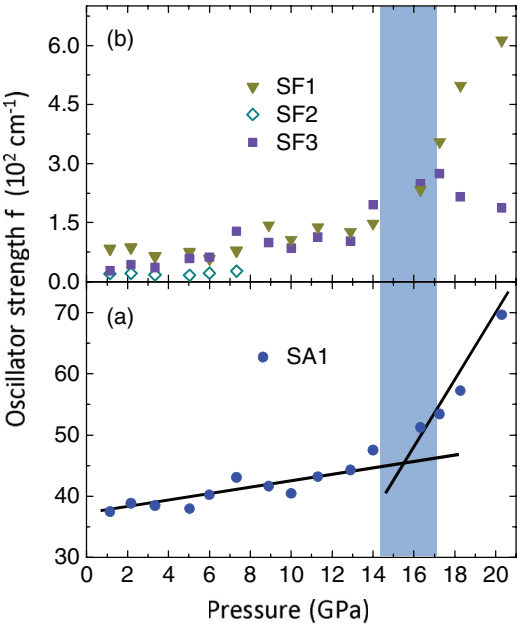

FIG. 8. (Color online) Oscillator strength of the observed *d-d* transitions of $CdCr_2O_4$. (a) Oscillator strength of the spin-allowed transition (SA1) increases with increasing pressure. (b) Oscillator strength of the spin-forbidden transitions (SF1, SF2, SF3), which is very small compared to the total oscillator strength. The shaded area marks the transition region and the black solid lines are guides to the eye.

be found, which broaden with increasing temperature and can no longer be completely resolved at room temperature [29], consistent with our data. We used Lorentz oscillators to describe the spin-allowed and spin-forbidden transitions at room temperature. The strong absorption band at $\omega_0 \approx 16\,760\ \mathrm{cm}^{-1}$ (SA1) shows a blueshift with increasing pressure, as shown in Fig. 7(b), but there is no significant frequency shift of the spin-forbidden excitations (SF1, SF2, SF3) up to 8 GPa. Above 8 GPa the three transitions are no longer distinguishable, and the curves are fitted with two overdamped absorption bands. An anomalous change in their central frequencies can be seen at 14 GPa [see Fig. 7(b)], followed by a blueshift on further pressure increase.

The oscillator strength of the excitations was calculated according to

$$f = \int_{\omega_1}^{\omega_2} A(\omega) d\omega, \qquad (2)$$

with the absorbance $A(\omega)$, $\omega_1 = 9000\ \mathrm{cm}^{-1}$, and $\omega_2 = 22\,000\ \mathrm{cm}^{-1}$. The oscillator strength of the spin-allowed transition increases with increasing pressure [see Fig. 8(a)]. Above $P_c \approx 16$ GPa the pressure-induced increase in oscillator strength is drastically enhanced. The three spin-forbidden transitions contribute very little to the total oscillator strength, but overall the oscillator strength of these features increases with pressure up to ≈15 GPa; at this pressure anomalies occur [see Fig. 8(b)].

In the far-infrared region we resolve two phonon modes [modes (1) and (2)] out of four predicted modes, since the other two low-frequency phonon modes are beyond the studied frequency range. For a more detailed discussion of the phonon modes and their evolution with pressure, we refer to Sec. IV. To extract the frequency, oscillator strength, and damping of the modes, the low-frequency reflectivity spectra were fitted with the Lorentz model. The illustration of the fit for three selected pressures for each compound and the so-obtained results for the fitting parameters are shown in Fig. 9.

For $ZnCr_2Se_4$ [see Fig. 9(d)] the phonon modes harden with increasing pressure. There is no significant change in damping and oscillator strength of both phonon modes up to $P \approx 10$ GPa. Above this pressure phonon mode (1) is no longer visible. By further increasing the pressure, the remaining mode (2) starts to lose its strength and broadens. At 14 GPa the phonon resonances can no longer be clearly resolved.

In the case of $HgCr_2S_4$, the two phonon modes harden with increasing pressure up to 12 GPa. Above 12 GPa mode (1) is no longer visible and mode (2) softens with increasing pressure. There is no significant change in oscillator strength of mode (1), but it starts to become more damped at around 8 GPa as shown in Fig. 9(e). With further increasing pressure the damping increases and mode (1) can no longer be resolved above 12 GPa. Mode (2) behaves differently, since there is no significant change in the damping up to 11 GPa. By further increasing the pressure the damping increases and also the oscillator strength of mode (2) increases. The phonon parameters show an anomaly at around 12 GPa [see Fig. 9(e)].

In $CdCr_2O_4$ the phonon modes harden with increasing pressure and there is no notable change in the oscillator strength of both modes (1) and (2) up to the highest measured pressure ($P \approx 14$ GPa) [see Fig. 9(f)]. Mode (1) loses intensity upon pressure application, but mode (2) shows only small modifications up to the highest measured pressure.

IV. DISCUSSION

The optical properties of Cr spinels have been extensively studied by various experimental methods. In the literature there are numerous Raman and infrared studies reporting about the phonon frequencies for various pure and mixed spinels. From the lattice symmetry of the normal spinels, the group

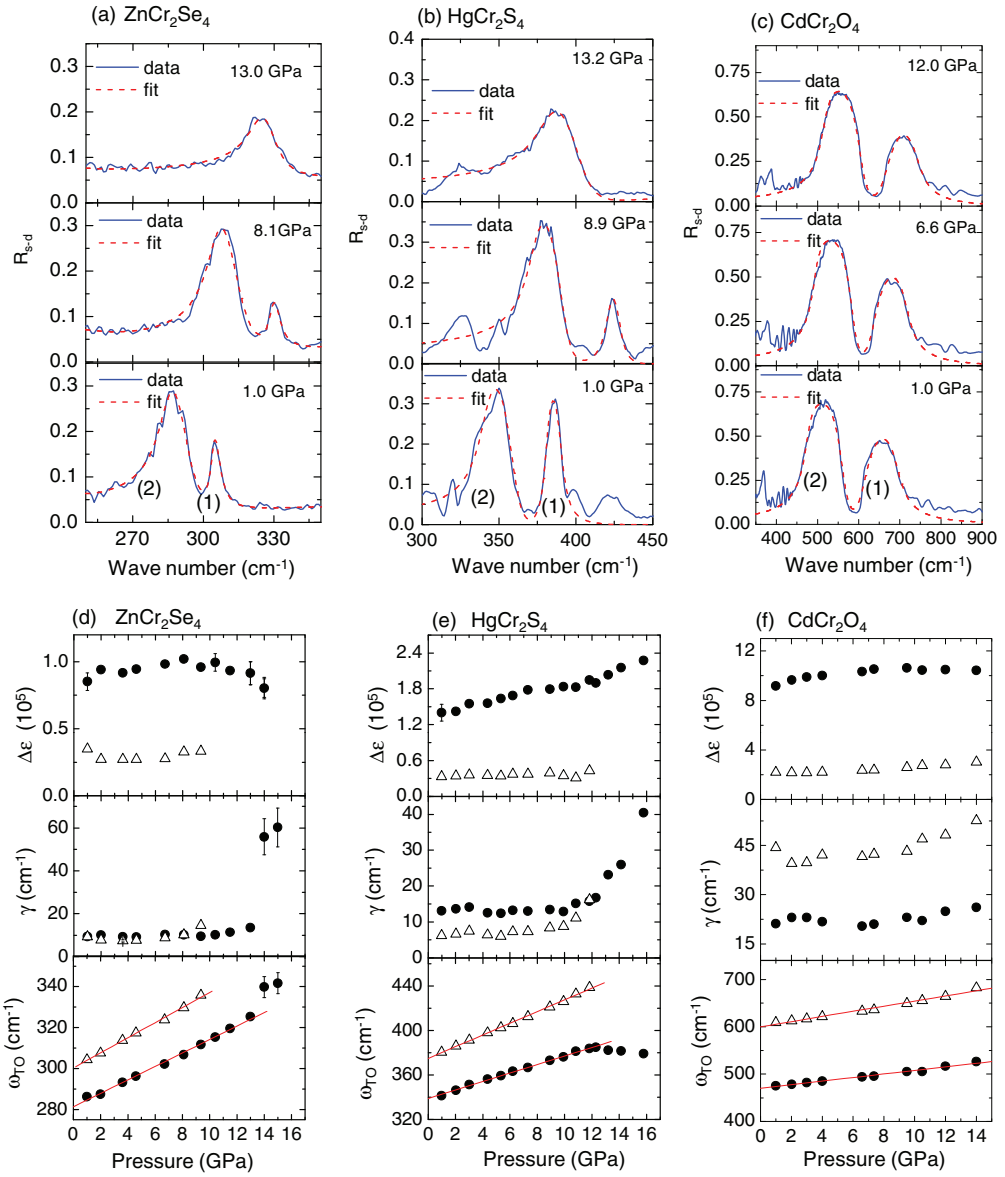

FIG. 9. (Color online) Illustration of the fit of two observed phonon modes denoted as (1) and (2) with the Lorentz model according to Eq. (1) for selected pressures for (a) $ZnCr_2Se_4$, (b) $HgCr_2S_4$, and (c) $CdCr_2O_4$. The obtained results from the fit are shown below for each compound [see (d)–(f)]. The pressure dependence of frequencies of optical phonons are fitted according to Eq. (3) to find the initial linear pressure coefficient.

theory analysis predicts four infrared-active triply degenerate T_{1u} phonon modes in the FIR spectrum [35]:

$$\begin{aligned}\Gamma &= 4T_{1u} && \text{(IR-active)}\\ &\quad + A_{1g} + E_{1g} + 3T_{2g} && \text{(Raman-active)}\\ &\quad + 2A_{2u} + 2E_u + T_{1g} + 2T_{2u} && \text{(silent)}.\end{aligned}$$

We have chosen to label the four IR-active modes as (1)–(4), starting from high to low frequencies. The origin of the T_{1u} modes has been the subject of controversy as two possible interpretations were proposed: In one case the two high-frequency phonon modes are related to the displacement of the Cr-X bond in the CrX_6 octahedra, while the two low-frequency phonon modes are related to the tetrahedra [16,36,37]. It has been shown experimentally [38–40] that the materials having an octahedral sublattice as one of the structural units exhibit phonon modes belonging to octahedral vibrations at higher frequencies compared to the other lattice vibrations.

On the other hand, Lutz and co-workers [41–46] claimed that almost all atoms contribute to the four IR-active phonon modes. They proposed that the contribution of A-site atoms to the higher-frequency phonon modes [modes (1) and (2)] is smaller compared to that to the two lower-frequency phonon modes. An assignment of the phonon modes to vibrations of tetrahedral AX_4, octahedral BX_6, or cubic B_4X_4 units of the structure is, within this framework, not possible [42]. However, one can hypothesize that for higher-frequency phonon modes the contribution of octahedral vibrations is larger compared to that of tetrahedral vibrations.

It has been predicted theoretically that in normal spinels the octahedral BX_6 unit is much more ionic than the tetrahedral

TABLE II. Values of the linear pressure coefficient C (cm^{-1}/GPa) for two phonon modes of the three investigated Cr-spinel compounds.

Compounds	Phonon mode (1)	Phonon mode (2)
$CdCr_2O_4$	5.41 ± 0.25	3.75 ± 0.17
$HgCr_2S_4$	5.25 ± 0.08	3.80 ± 0.06
$ZnCr_2Se_4$	3.68 ± 0.10	3.28 ± 0.07

AX_4, and the value of the force constant for Cr-X is larger than that of A-X [43,44]. In infrared experiments the oscillator strength is directly related to the ionicity of a bond [47]. The more ionic the character of the bond is, the stronger will be the vibrational mode belonging to that bond. Mode (2) is stronger compared to mode (1), indicating a larger contribution of BX_6 octahedra [see Figs. 9(d)–9(f)]. Furthermore, the mode intensities decrease moving from the oxide over the sulfide to the selenides, which suggests an increasing covalency of the bonds [1].

With increasing pressure all phonon modes shift to higher frequencies in a linear fashion [see Figs. 9(d)–9(f)]. The linear pressure coefficient C in the low-pressure regime was obtained by fitting the frequency of the phonon modes with the following equation:

$$\omega(P) = \omega_o + C\,P, \tag{3}$$

where P is the applied pressure, ω_o is the phonon frequency at zero pressure, and C is the linear pressure coefficient. The obtained results are given in Table II. The value of C represents the stiffness of bonds, and therefore can serve as a measure for the compressibility of the compound. In all investigated Cr-spinel compounds, the value of C for mode (2) is smaller compared to mode (1), which attributes to the fact that the respective bonding of mode (2) is stiffer compared to mode (1). Moreover, the C values for the phonon modes of $CdCr_2O_4$ and $HgCr_2S_4$ are larger than those of $ZnCr_2Se_4$.

Regarding the compressibility difference for the three investigated compounds, the foremost consideration is the part of the unit cell volume, which is mainly occupied by anions. The compressibility is mainly determined by the X sublattice [3,15], since the number of X-X bonds is larger compared to the other bonds (i.e., Cr-X and A-X bonds). In the periodic table, the electronegativity decreases from oxygen to selenium, while the size of the ions increases. The selenium (Se^{2-}) ion is bigger as compared to sulfur (S^{2-}) and oxygen (O^{2-}) and this corresponds to a larger bond length of chalcogenides compared to oxides. Application of external pressure will affect the longer bond length more strongly than the shorter bond length. With these considerations, the chalcogenides are expected to be more compressible as compared to the oxides. The higher compressibility corresponds to a more covalent character of the chemical bond and a lower ionicity of the anions [3]. $ZnCr_2Se_4$ shows a semiconducting character, while $CdCr_2O_4$ shows insulating behavior as covalency increases from the oxide to the selenide. In this respect, the rather small values of the linear pressure coefficient C for the modes in $ZnCr_2Se_4$ are surprising.

For the investigated chalcogenide compounds the phonon parameters exhibit anomalies in their pressure dependence:

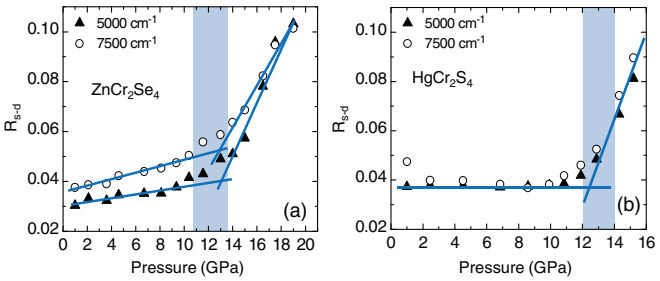

FIG. 10. (Color online) Estimation of P_c for (a) $ZnCr_2Se_4$ and (b) $HgCr_2S_4$ by plotting the change in reflectivity $R_{s\text{-}d}$ level with increasing pressure at 5000 and 7500 cm^{-1}, shown with solid triangles and open circles, respectively. The shaded areas mark the transition region and the solid lines are guides to the eye.

For $ZnCr_2Se_4$ anomalies occur at $P_c \approx 10$ GPa, which are interpreted in terms of a structural phase transition from cubic to tetragonal symmetry. This is supported by an x-ray powder diffraction study [3] where a pressure-induced structural phase transformation from cubic ($Fd\bar{3}m$) to tetragonal ($I\bar{4}$) was reported for $CdCr_2Se_4$ at around 10 GPa. The phonon parameters of $HgCr_2S_4$ show an anomaly at around 12 GPa, which is supported by a very recent Raman study of $HgCr_2S_4$ under pressure. A splitting of vibrational Raman modes was observed starting at around 12 GPa and related to a structural phase transition from a cubic to a tetragonal symmetry observed by diffraction methods [48]. The compressibility of oxides is low compared to the chalcogenides, since the chemical bonds are very stiff, and therefore the critical pressure is expected to be higher. Indeed, a Raman study of $ZnCr_2O_4$ under pressure reveals a sluggish structural phase transition starting at 17.5 GPa, which is completed at around 35 GPa [49]. Consistent with this finding is the absence of an anomaly for the phonon modes in $CdCr_2O_4$ up to 14.0 GPa, according to our data.

Signatures of the pressure-induced structural phase transition are also expected in the pressure evolution of the electronic excitations. Therefore, we plot in Fig. 10 the change in the reflectivity spectra as a function of pressure at 5000 and 7500 cm^{-1} for $ZnCr_2Se_4$ and $HgCr_2S_4$, since the reflectivity in this range relates to the electronic excitations in the materials. For $ZnCr_2Se_4$ the reflectivity versus pressure curve shows a continuous increase in R_{s-d} with increasing pressure up to 10 GPa. By further increasing pressure there is a drastic increase in $R_{s\text{-}d}$, indicating that the new structural phase is more susceptible to external pressure. In the case of $HgCr_2S_4$ there is a drastic increase in $R_{s\text{-}d}$ above 12 GPa; below this pressure the reflectivity level remains almost constant at selected frequencies [see Fig. 10(b)]. $CdCr_2O_4$ shows an anomaly in the oscillator strength of the CF excitations at $P_c \approx$ 15 GPa [see Figs. 7(b) and 8]. A higher value of the critical pressure for $CdCr_2O_4$ as compared to the chalcogenides is consistent with our low-frequency results.

V. SUMMARY

The Cr-spinel compounds $ZnCr_2Se_4$, $HgCr_2S_4$, and $CdCr_2O_4$ were studied by optical spectroscopy under pressure. With increasing pressure all observed phonon modes shift linearly to higher frequencies in the low-pressure regime.

For $ZnCr_2Se_4$ and $HgCr_2S_4$ the electronic excitations exhibit a redshift upon pressure application, whereas for $CdCr_2O_4$ they show a blueshift. According to the anomalies found in the phonon behavior, reflectivity level, and the electronic excitations, all three compounds undergo a pressure-induced structural phase transition with the critical pressure $P_c \approx 10$, 12, and 15 GPa for $ZnCr_2Se_4$, $HgCr_2S_4$, and $CdCr_2O_4$, respectively.

ACKNOWLEDGMENTS

We acknowledge the ANKA Angströmquelle Karlsruhe for the provision of beamtime and thank B. Gasharova, Y.-L. Mathis, D. Moss, and M. Süpfle for assistance in using the beamline ANKA-IR. Financial support by the Bayerische Forschungsstiftung and the DFG (Emmy Noether-program, SFB 484, TRR 80) is acknowledged.

[1] T. Rudolf, Ch. Kant, F. Mayr, J. Hemberger, V. Tsurkan, and A. Loidl, New J. Phys. **9**, 76 (2007).
[2] S.-H. Lee, C. Broholm, W. Ratcliff, G. Gasparovic, Q. Huang, T. H. Kim, and S.-W. Cheong, Nature (London) **418**, 856 (2002).
[3] A. Waśkowska, L. Gerward, J. Staun Olsen, and E. Malicka, J. Phys.: Condens. Matter. **14**, 12423 (2002).
[4] J. Hemberger, P. Lunkenheimer, R. Ficht, H.-A. Krug von Nidda, V. Tsurkan, and A. Loidl, Nature (London) **434**, 364 (2005).
[5] G. Xu, H. Weng, Z. Wang, X. Dai, and Z. Fang, Phys. Rev. Lett. **107**, 186806 (2011).
[6] Y. Yamashita and K. Ueda, Phys. Rev. Lett. **85**, 4960 (2000).
[7] O. Tchernyshyov, R. Moessner, and S. L. Sondhi, Phys. Rev. Lett. **88**, 067203 (2002).
[8] T. Watanabe, J. Phys. Soc. Jpn. **37**, 140 (1974).
[9] Ch. Kant, J. Deisenhofer, T. Rudolf, F. Mayr, F. Schrettle, A. Loidl, V. Gnezdilov, D. Wulferding, P. Lemmens, and V. Tsurkan, Phys. Rev. B. **80**, 214417 (2009).
[10] T. Rudolf, Ch. Kant, F. Mayr, M. Schmidt, V. Tsurkan, J. Deisenhofer, and A. Loidl, Eur. Phys. J. B **68**, 153 (2009).
[11] R. Valdes Aguilar, A. B. Sushkov, Y. J. Choi, S.-W. Cheong, and H. D. Drew, Phys. Rev. B **77**, 092412 (2008).
[12] S. Massidda, M. Posternak, A. Baldereschi, and R. Resta, Phys. Rev. Lett. **82**, 430 (1999).
[13] Ch. Kant, M. Schmidt, Z. Wang, F. Mayr, V. Tsurkan, J. Deisenhofer, and A. Loidl, Phys. Rev. Lett. **108**, 177203 (2012).
[14] H. D. Lutz, G. Wäschenbach, G. Kliche, and H. Haeuseler, J. Solid State Chem. **48**, 196 (1983).
[15] A. Waśkowska, L. Gerward, J. Staun Olsen, M. Feliz, R. Llusar, L. Gracia, M. Marqúes, and J. M. Recio, J. Phys.: Condens. Matter **16**, 53 (2004).
[16] T. Rudolf, Ch. Kant, F. Mayr, J. Hemberger, V. Tsurkan, and A. Loidl, Phys. Rev. B **75**, 052410 (2007).
[17] G. Huber, K. Syassen, and W. B. Holzapfel, Phys. Rev. B **15**, 5123 (1977).
[18] H. K. Mao, J. Xu, and P. M. Bell, J. Geophys. Res. **91**, 4673 (1986).
[19] F. Gervais, in *Infrared and Millimeter Waves*, edited by K. J. Button (Academic, New York, 1983).
[20] N. W. Ashcroft and N. D. Mermin, *Solid State Physics* (Harcourt Brace College Publishers, Fort Worth, TX, 1976).
[21] F. Birch, J. Geophys. Res. **83**, 1257 (1978).
[22] W. B. Holzapfel, Rep. Prog. Phys. **59**, 29 (1996).
[23] J. S. Plaskett and P. N. Schatz, J. Chem. Phys. **38**, 612 (1963).
[24] A. Pashkin, M. Dressel, and C. A. Kuntscher, Phys. Rev. B **74**, 165118 (2006).
[25] A. D. Liehr, J. Phys. Chem. **67**, 1314 (1963).
[26] B. N. Figgis and M. A. Hitchman, *Ligand Field Theory and its Applications* (Wiley-VCH, New York, 1999).
[27] K. Ohgushi, Y. Okimoto, T. Ogasawara, S. Miyasaka, and Y. Tokura, J. Phys. Soc. Jpn. **77**, 034713 (2008).
[28] C. K. Jorgensen, Inorg. Chem. Acta Rev. **2**, 65 (1968).
[29] M. Schmidt, Z. Wang, Ch. Kant, F. Mayr, S. Toth, A. T. M. N. Islam, B. Lake, V. Tsurkan, A. Loidl, and J. Deisenhofer, Phys. Rev. B **87**, 224424 (2013).
[30] P. K. Larsen and S. Wittekoek, Phys. Rev. Lett. **29**, 1597 (1972).
[31] L. L. Golik, Z. E. Kunkova, T. G. Aminov, and G. G. Shabunina, Fizika Tverdogo Tela **38**, 1295 (1996).
[32] S. Sugano, Y. Tanabe, and H. Kamimura, *Multiplets of Transition-Metal Ions in Crystals* (Academic, New York, 1970).
[33] C. A. Kuntscher, A. Pashkin, H. Hoffmann, S. Frank, M. Klemm, S. Horn, A. Schönleber, S. van Smaalen, M. Hanfland, S. Glawion, M. Sing, and R. Claessen, Phys. Rev. B **78**, 035106 (2008).
[34] M. Taniguchi, A. Fujimori, and S. Suga, Solid State Commun. **70**, 191 (1989).
[35] K. Wakamura, T. Arai, and K. Kudo, J. Phys. Soc. Jpn. **40**, 1118 (1976).
[36] D. Basak and J. Ghose, Spectrochim. Acta A **50**, 713 (1994).
[37] C. J. Fennie and K. M. Rabe, Phys. Rev. B **72**, 214123 (2005).
[38] K. Thirunavukkuarasu, F. Lichtenberg, and C. A. Kuntscher, J. Phys.: Condens. Matter **18**, 9173 (2006).
[39] R. Haumont, P. Bouvier, A. Pashkin, K. Rabia, S. Frank, B. Dkhil, W. A. Crichton, C. A. Kuntscher, and J. Kreisel, Phys. Rev. B **79**, 184110 (2009).
[40] J. Preudhomme and P. Tarte, Spectrochim. Acta A **27**, 1817 (1971).
[41] H. D. Lutz and H. Haeuseler, J. Mol. Struct. **511–512**, 69 (1999).
[42] H. D. Lutz, J. Himmrich, and J. Haeuseler, Z. Naturforsch., A: Phys. Sci. **45**, 893 (1990).
[43] J. Zwinscher and H. D. Lutz, J. Solid State Chem. **118**, 43 (1995).
[44] J. Zwinscher and H. D. Lutz, J. Alloys Compd. **219**, 103 (1995).
[45] C. Kringe, B. Oft, V. Schellenschläger, and H. D. Lutz, J. Mol. Struct. **596**, 25 (2001).
[46] J. Himmrich and H. D. Lutz, J. Solid State Commun. **79**, 447 (1991).
[47] K. Wakamura and T. Arai, Phase Transitions **27**, 129 (1990).
[48] I. Efthimiopoulos, A. Yaresko, V. Tsurkan, J. Deisenhofer, A. Loidl, C. Park, and Y. Wang, Appl. Phys. Lett. **103**, 201908 (2013).
[49] Z. Wang, P. Lazor, and G. Artioli, J. Solid State Chem. **165**, 165 (2002).